Mitigating Summertime Marine Heatwaves via Targeted Marine Cloud Brightening

Matthew T. Luongo[1,2*], Edward Blanchard-Wrigglesworth[3], Kyle C. Armour[2,3], Haruki Hirasawa[3], Jacob T. Cohen[1,4], & Aaron Donohoe[3,5]

1. Cooperative Institute for Climate, Ocean, & Ecosystem Studies, University of Washington, Seattle, WA, USA
2. School of Oceanography, University of Washington, Seattle, WA, USA
3. Department of Atmospheric & Climate Science, University of Washington, Seattle, WA, USA
4. NOAA Pacific Marine Environmental Laboratory, Seattle, WA, USA
5. Applied Physics Laboratory, University of Washington, Seattle, WA, USA

* Corresponding author: mluongo@uw.edu

Mitigating Summertime Marine Heatwaves via Targeted Marine Cloud Brightening

Matthew T. Luongo[1,2*], Edward Blanchard-Wrigglesworth[3], Kyle C. Armour[2,3], Haruki Hirasawa[3], Jacob T. Cohen[1,4], Aaron Donohoe[3,5]

[1]Cooperative Institute for Climate, Ocean, & Ecosystem Studies, University of Washington, Seattle, WA, USA.
[2]School of Oceanography, University of Washington, Seattle, WA, USA.
[3]Department of Atmospheric & Climate Science, University of Washington, Seattle, WA, USA.
[4]NOAA Pacific Marine Environmental Laboratory, Seattle, WA, USA.
[5]Applied Physics Laboratory, University of Washington, Seattle, WA, USA.

*Corresponding author(s). E-mail(s): mluongo@uw.edu;

Abstract

Marine heatwaves (MHWs) negatively impact marine ecosystems and coastal economies. Here, we evaluate whether a preemptive, short-term, localized surface emission of sea salt aerosols (marine cloud brightening, MCB) can mitigate the impacts of a predicted MHW without creating significant effects beyond the intervention zone. As a case study, we apply MCB to the 2019 Northeast Pacific MHW, "The Blob 2.0," using a global climate model seasonal-to-multiyear predictability ensemble. Initiating MCB in May 2019 mitigates important negative consequences of the event, substantially reducing the MHW magnitude and limiting associated declines in surface oxygen. The impacts of this intervention are mostly local and limited to summer, even when MCB is extended into winter, with nonlocal climate effects smaller than internal variability. By demonstrating local efficacy and minor remote impacts for mitigating the Blob 2.0, this work motivates further study of whether localized and temporary climate interventions can safely and effectively mitigate MHWs.

Keywords: Marine Heatwaves, Marine Cloud Brightening, Seasonal Predictability, Extreme Events

1 Introduction

Persistent periods of extremely warm sea surface temperatures (SSTs), known as marine heatwaves (MHWs) [1, 2], can have profound impacts on marine ecosystems [3–5], fisheries [4, 6, 7], biogeochemistry [8–10], and coastal economies [7, 11]. As anthropogenic greenhouse gas emissions have warmed the oceans, MHWs have become longer-lasting and more frequent [12, 13] – a trend that is expected to continue with ongoing global temperature rise [12, 14, 15].

The mid-latitude Northeast Pacific stands out as a hot spot for observed [12, 13, 16] and projected [12, 15] MHWs. For example, between 2013 and 2016, the Northeast Pacific experienced extraordinarily warm, winter-intensified SSTs (known as "The Blob" [17]) causing geographic shifts of species, fisheries closures, and mass strandings of marine mammals and birds along the North American west coast [4]. Half a decade later, in summer 2019, another Northeast Pacific MHW (known as "The Blob 2.0" [18–20]) substantially impacted marine ecosystems, biogeochemistry, and fisheries in the region [5, 9, 11, 21].

To allow decision makers and industries to plan for and respond to MHWs, prior work has highlighted their predictability. For example, Northeast Pacific MHWs can be skillfully predicted several months in advance using global climate model (GCM) ensemble forecasts [e.g., 22, 23]. In this work, we leverage this predictability to evaluate the extent to which a preemptive, short-term, localized climate intervention can mitigate the regional impacts of a forecast MHW without creating adverse remote effects. Specifically, we perform GCM simulations to evaluate whether a localized and temporary lower tropospheric emission of sea salt aerosols (i.e., marine cloud brightening: MCB [24, 25]) can reduce the magnitude of a summertime MHW.

By directly reflecting solar radiation and, more importantly, serving as cloud condensation nuclei to enhance cloud albedo via the Twomey effect, MCB via sea salt aerosol emission has been largely proposed as a long-term and large-scale climate intervention strategy to produce planetary-scale cooling to offset anthropogenic global warming [26–29]. Many studies [27–33] have simulated MCB using GCMs and focused on the global impacts of long-term MCB in subtropical stratocumulus decks. Sustained MCB in these regions produces globally inhomogeneous patterns of cooling that do not necessarily cancel greenhouse-gas-driven warming. For example, MCB in the subtropical Southeast Pacific triggers a long-term La Niña-like response that drives unintended, and potentially adverse, global climate effects through tropical-to-extratropical teleconnections [27–31, 33, 34].

A handful of studies have proposed more regionally-targeted, but still long-term, MCB approaches intended to reduce certain regional climate change impacts, such as Great Barrier Reef coral bleaching [30, 35], polar sea ice loss [30, 36], or increased heat stress over land [32]. Owing to their long-term nature, these MCB perturbations often still produce significant and unintended climate effects across the globe. Recently, Wan et al. [37] considered how targeted MCB could affect shorter timescale (interannual) climate events by showing that Southeast Pacific MCB can weaken a subsequent El Niño event if deployed early enough. Nevertheless, by affecting the tropical Pacific, this simulated intervention drove significant global impacts and changed the temporal trajectory and magnitude of the subsequent La Niña.

Here, we explore the novel question of whether a preemptive, short-term (seasonal-to-yearlong), localized MCB intervention can prevent the negative local impacts of an extreme summertime MHW event. We use the 2019 Northeast Pacific Blob 2.0 as a case study due to its substantial magnitude [18–20] and ecological [5, 9, 21] and socioeconomic impacts [11]. We further evaluate whether such a targeted intervention could be done while avoiding significant remote climate effects beyond the intervention zone.

2 Targeted MCB Mitigates Regional Summertime Impacts of the Blob 2.0

The summer 2019 Blob 2.0 MHW was characterized by local SST anomalies of $2-2.5°$C (thick red line in Fig. 1a, [18–21]) in a region that stretches from the California Bight to the Gulf of Alaska and 160°W to the North American west coast. This MHW was principally caused by a regional weakening of winds which reduced evaporative cooling and upper ocean mixing; positive cloud feedbacks then reinforced warming [18].

The predictability of large MHWs like the Blob 2.0 derives from local persistence and evolution of ocean heat content anomalies and remote temperature impacts on large-scale atmospheric circulation [22]. As such, GCM predictability ensembles initialized with observationally-informed three-dimensional oceanic conditions, such as the Seasonal-to-Multiyear Large Ensemble (SMYLE [39], Methods), show substantial skill in predicting the magnitude and location of observed MHWs [23]. For example, when initialized on May 1, 2019, nearly all SMYLE ensemble members predict anomalously warm SSTs through summer 2019 in the observed Blob 2.0 region (thin black lines in Fig. 1a and maps in Extended Data Fig. 1). The ensemble mean SST anomaly (thick black line in Fig. 1a) nearly matches the SMYLE historical 90^{th} percentile SST anomaly (brown line in Fig. 1a), indicating a successful prediction of a MHW at this approximate time and location. This predictive skill arises because the May 1, 2019 ocean is preconditioned to experience a summer MHW; that skill exceeds simple damped persistence of SSTs (medium dashed red line in Fig. 1a). Although the SMYLE ensemble mean SST anomaly is smaller than that observed for the event, individual ensemble members predict SST anomalies as high as 2°C, substantially higher than the 90^{th} percentile MHW threshold and near the observed MHW magnitude. We use this SMYLE ensemble as the control ("Ctrl") against which our ensemble of MCB intervention simulations is compared.

We simulate MCB by emitting a steady surface flux of 0.0417 Tg of sea salt aerosol per month from May 1, 2019 through September 30, 2019 in the Gulf of Alaska region (Extended Data Fig. 2a and black rectangles in Fig. 2) within 20 ensemble members that are otherwise identical to the Ctrl ensemble (thin light blue lines in Fig. 1b). We select the aerosol emission region (our "intervention zone") as the approximate location with largest June-July-August (JJA) average ensemble mean SST anomalies in Ctrl, thus representing the region predicted to have the most extreme MHW (Fig. 2a). We evaluate two aerosol emission rates (Methods) and primarily present the lower rate throughout our analysis (referred to as "MCB_{Low}").

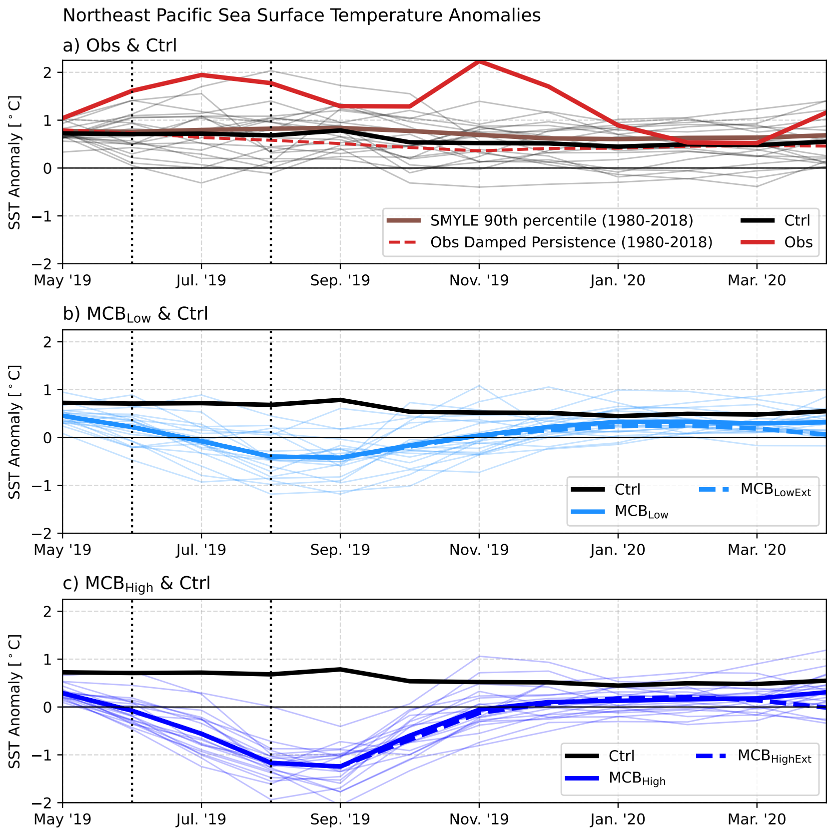

Fig. 1 May 2019 through April 2020 time series of Northeast Pacific intervention zone area-averaged ($40-50°$N, $155-135°$W) sea surface temperature (SST) anomalies for a) GODAS observations ([38], solid red line), Ctrl ensemble members (thin solid black lines), Ctrl ensemble mean (thick solid black line), damped SST persistence forecast from observations (medium dashed red line), and SMYLE 90^{th} percentile SST threshold (thick solid brown line); b) MCB_{Low} ensemble members (thin solid light blue lines), MCB_{Low} ensemble mean (thick solid light blue line), MCB_{LowExt} ensemble mean (thick dashed light blue line), and Ctrl ensemble mean; and c) MCB_{High} ensemble members (thin solid dark blue lines), MCB_{High} ensemble mean (thick solid dark blue line), $MCB_{HighExt}$ ensemble mean (thick dashed dark blue line), and Ctrl ensemble mean. Observed SST anomalies are monthly averages calculated with respect to the observed 1980 through 2018 monthly climatology [18]. Model-derived SST anomalies are monthly averages calculated with respect to all SMYLE ensemble members initialized on May 1 from 1980 through 2018 [22]. Thin dotted lines in each panel are plotted at June 15, 2019 and August 15, 2019 to highlight summer 2019. Note that the monthly-averaged May 2019 value of MCB_{Low}, MCB_{LowExt}, MCB_{High}, and $MCB_{HighExt}$ have already diverged from Ctrl after several weeks of MCB forcing.

The ensemble mean JJA SST response of MCB_{Low} averaged over the intervention zone is 0.79°C cooler than Ctrl (Fig. 1b & 2b-c), fully mitigating the forecast MHW. In fact, all MCB_{Low} ensemble members show JJA SST anomalies below the Ctrl ensemble mean, demonstrating that MCB effectively mitigates this MHW even when accounting for internal variability. The MCB intervention also mitigates the predicted negative surface dissolved oxygen (DO) anomaly that is coincident with the MHW (Fig. 2d-f).

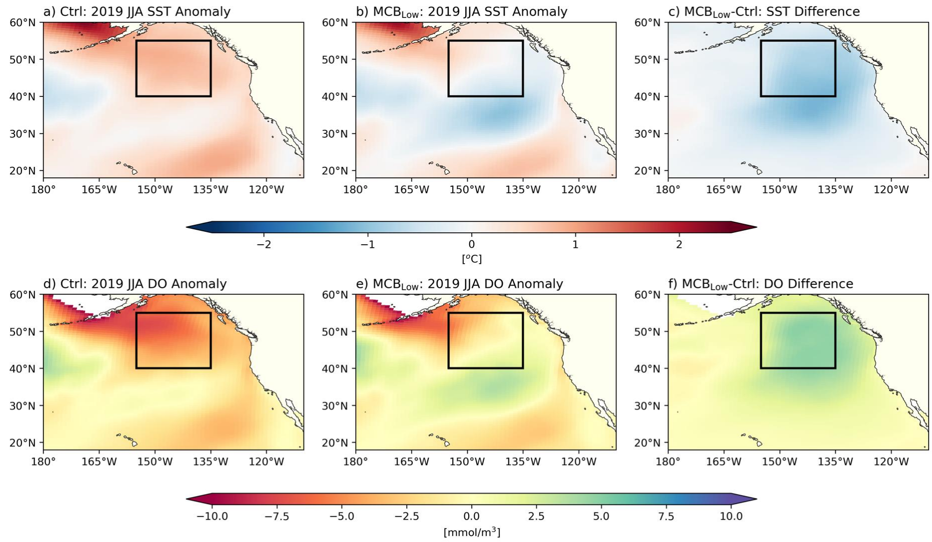

Fig. 2 Top row: 2019 June-July-August (JJA) sea surface temperature (SST) anomaly in a) Ctrl, b) MCB$_{\text{Low}}$, and c) MCB$_{\text{Low}}$-Ctrl. Bottom row: 2019 JJA surface dissolved oxygen (DO) anomaly in d) Ctrl, e) MCB$_{\text{Low}}$, and f) MCB$_{\text{Low}}$-Ctrl. Anomalies are calculated relative to all SMYLE simulations initialized on May 1 from 1980 through 2018. Black rectangles denote the intervention zone region in the Gulf of Alaska over which the MCB intervention is applied.

2.1 Drivers of the Regional Summertime Response to MCB

These cooled SSTs illustrate the physical motivation behind MCB: a surface flux of sea salt aerosol (Extended Data Fig. 2a) creates a regional increase in lower tropospheric cloud condensation nuclei (Extended Data Fig. 2b), leading to an increase in cloud droplet concentration (Extended Data Fig. 2c), which increases cloud albedo via the Twomey effect to reflect incoming shortwave radiation (Fig. 3a). An area-averaged surface heat budget (Fig. 3e) reveals that the JJA intervention-zone-average reduction in net surface shortwave radiation (-28.6 Wm^{-2}, relative to Ctrl) is the primary driver of the change in net surface heat flux (-18.9 Wm^{-2}) and thus more than sufficient to explain the anomalous surface and upper ocean cooling. This reduction in solar radiation due to MCB is mostly due to the indirect aerosol effect, which causes a large shortwave cloud forcing (Fig. 3c, -25.2 Wm^{-2}), while the reduction from direct solar reflection by aerosols is much smaller (-3.4 Wm^{-2}). Modest decreases in net upward longwave radiation and turbulent heat fluxes from the surface to the atmosphere damp this cooling (Fig. 3b, $+9.7$ Wm^{-2}) and mirror the spatial pattern of SST, suggesting that reduced longwave and turbulent loss to the atmosphere is itself a response to SST cooling.

The cooler and more oxygenated waters driven by MCB extend eastward and southward beyond the intervention zone over JJA (Fig. 2c & f), with the largest anomalies in the southeast section of the intervention zone and extending southwest

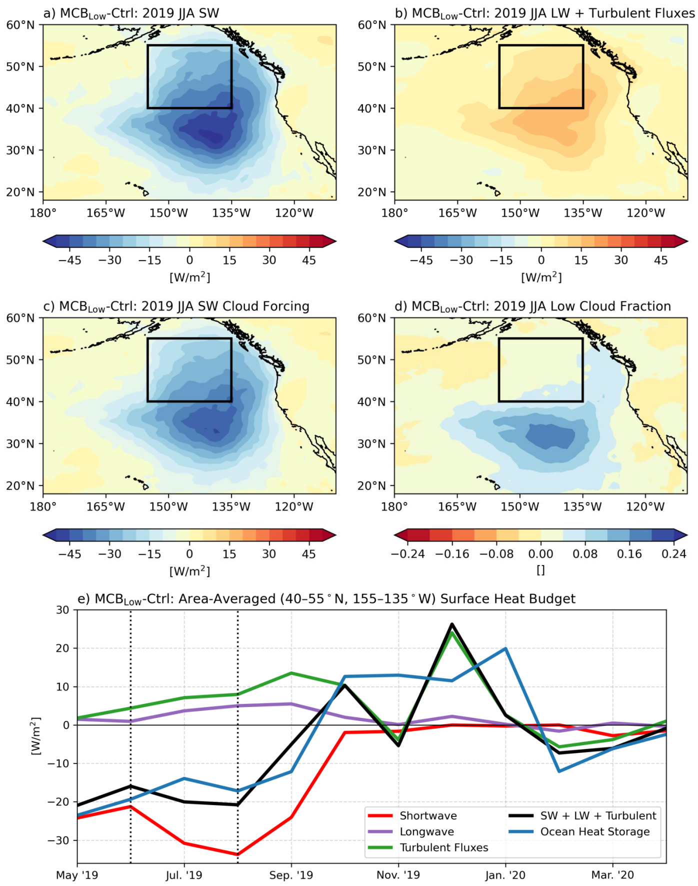

Fig. 3 Top two rows: 2019 June-July-August (JJA) $\mathrm{MCB_{Low}}$-Ctrl difference in a) net surface shortwave radiation (SW), b) the sum of net surface longwave radiation (LW) and latent and sensible turbulent heat fluxes, c) net surface shortwave radiation due to cloud forcing, and d) low cloud fraction. Radiative fluxes in a)-c) are defined as positive downward (i.e. into the ocean). Black rectangles denote the intervention zone region in the Gulf of Alaska over which the MCB intervention is applied. Bottom row: Intervention zone area-averaged ($40-50°$N, $155-135°$W) surface heat budget from May 2019 through April 2020 for $\mathrm{MCB_{Low}}$-Ctrl. Thin vertical dotted lines demark June 15, 2019 and August 15, 2019.

toward Hawaii. The shape of these anomalies indicate a role for North Pacific anticyclonic (clockwise) winds [32, 40] which advect both cooled air and sea salt (serving as cloud condensation nuclei) southward from the intervention zone (Extended Data Fig. 2b). As a result, the largest MCB effects (amounting to a surface energy budget anomaly of ~ -45 Wm^{-2} over JJA) are realized just south of the intervention zone: advection of cold air strengthens the near-surface temperature inversion to create more low clouds (Fig. 3d) and advection of aerosols creates brighter clouds (Extended Data Fig. 2c). Cooler temperatures in the subtropical stratocumulus deck are then amplified by the positive low-cloud-SST feedback [40].

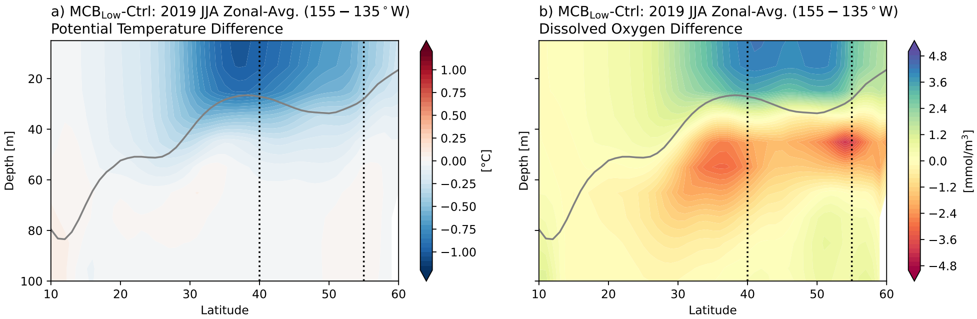

Fig. 4 2019 June-July-August (JJA) MCB$_{Low}$-Ctrl difference in zonally-averaged (155 − 135°W) subsurface a) potential temperature and b) dissolved oxygen. The solid gray line is the JJA climatological mixed layer depth calculated from SMYLE over 1980 through 2018. Dotted vertical lines denote the intervention zone latitudes.

Zonal-mean subsurface potential temperature anomalies are spatially co-located with the strongest change in SST and cloud forcing (Fig. 4a). Additionally, they are largely confined to the seasonally-evolving mixed layer, suggesting that these anomalies have not subducted into the permanent thermocline over JJA.

Whereas the JJA SST and surface DO responses exhibit similar anomaly patterns (Fig. 2c & f), subsurface DO anomalies exhibit a markedly different structure than potential temperature. Within the climatological mixed layer there is an increase in DO (Fig. 4b), likely due to increased gas solubility at lower temperatures [10]. However, MCB causes a DO decrease beneath the climatological mixed layer. While past work has shown baroclinic DO responses to volcanic cooling [41], these changes were tied to deeper mode water ventilation. Instead, this summertime reduction in DO beneath the mixed layer but within the photic zone results from a reduction in photosynthesis (Extended Data Fig. 3), and thus DO production, likely due to MCB-reduced solar forcing (Fig. 3a).

2.2 Seasonal Structure of the Response to MCB

The MCB$_{Low}$ emission of sea salt aerosol slightly overcorrects the forecast ensemble mean MHW, leading to anomalously cool SSTs in summer 2019 (Fig. 1b). However, this overcorrection is short-lived: after peaking in September 2019, the ensemble mean MCB$_{Low}$ local SST anomaly erodes to zero by November 2019 and then becomes anomalously warm, but still lower than the Ctrl ensemble mean, through April 2020. A key question is why the response to MCB appears to be limited to summer months – is it because MCB$_{Low}$ aerosol emissions cease at the end of September 2019 or is it moderated by some aspect of the seasonal cycle?

To explore this, we perform three additional 20-member MCB ensembles: one in which the sea salt emissions of MCB$_{Low}$ are extended through April 2020 ("MCB$_{LowExt}$"), one in which the emissions magnitude is quintupled but still ceased in September 2019 ("MCB$_{High}$"), and one in which the emissions magnitude is quintupled and extended through April 2020 ("MCB$_{HighExt}$"). MCB$_{High}$ produces larger cooling during summer 2019 (Fig. 1c). However, in all four sets of simulations, the MCB ensembles become indistinguishable from the Ctrl ensemble in the intervention zone after November 2019. Therefore, the reduction in the local SST response of MCB_{Low} beyond summer 2019 is not due to a relatively low emissions magnitude or cessation of emissions. Rather, it is due to the arrival of winter in the Gulf of Alaska: the seasonal reduction in solar insolation limits the wintertime impact of cloud forcing, increased wintertime winds increase turbulent damping, and a deeper wintertime mixed layer develops.

Thus, the regional seasonal cycle serves as a natural brake on local impacts of the summertime MCB intervention: even with overly-strong summertime cooling or extended sea salt aerosol emission, impacts do not persist locally past early fall. This detail can shape strategy for short-term deployments. For example, continuing mid-latitude aerosol emission past boreal autumn is ineffective as there is no significant difference between MCB_{Low} and MCB_{LowExt}.

3 Remote Impacts of MCB

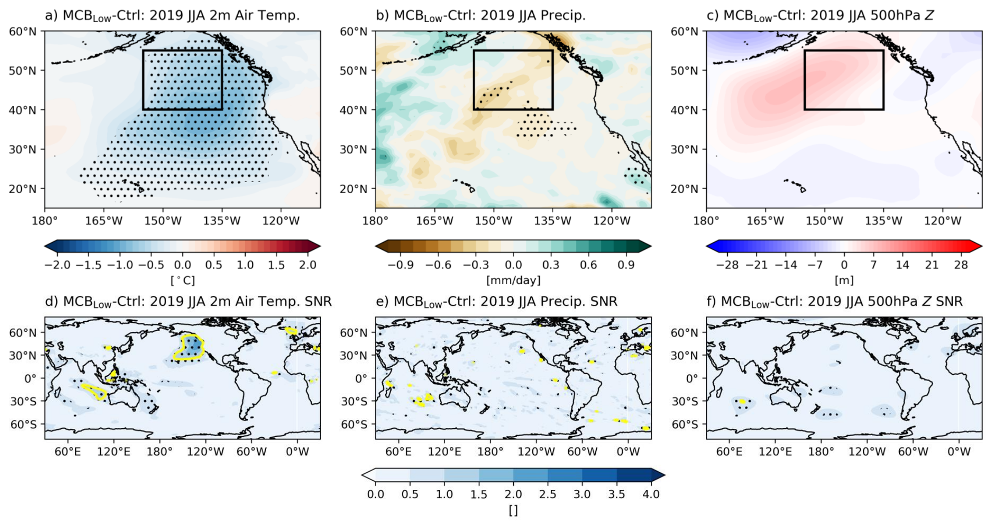

Fig. 5 Top row: 2019 June-July-August (JJA) MCB_{Low}-Ctrl difference in a) 2m (near-surface) air temperature, b) precipitation, and c) 500 hPa geopotential height (Z). Stippled regions are significant with 95% confidence. Black rectangles denote the intervention zone region in the Gulf of Alaska over which the MCB intervention is applied. Bottom row: Global map of JJA MCB_{Low}-Ctrl signal-to-noise ratio (SNR) for d) 2m air temperature, e) precipitation, and f) 500 hPa Z. Stippled regions are significant with 95% confidence. The SNR = 1 contour is highlighted in yellow.

Coupled feedbacks between the ocean and atmosphere allow MHW impacts to remotely affect land and sea temperatures over great distances [42–44]. Similarly, MCB-cooled SST anomalies can drive remote responses through those same teleconnections [27–29, 45]. However, even in the presence of MCB, internal variability substantially shapes each member's climate response (Extended Data Fig. 4). Thus, to determine the remote impact of our intervention, we consider ensemble spread in addition to ensemble mean differences.

To measure the statistical significance of the effects of MCB, we consider whether the difference between the MCB and Ctrl ensemble means is detectable relative to internal climate variability (Methods). The only coherent statistically significant difference between MCB_{Low} and Ctrl ensemble mean JJA near-surface air temperature occurs over the Gulf of Alaska (Fig. 5a & d). Except for slight drying in and near the intervention zone, other atmospheric phenomena, such as precipitation (Fig. 5b & e) and 500 hPa geopotential height (Fig. 5c & f), do not show widespread significant responses to MCB_{Low}. In addition, the emitted particles primarily remain over the ocean (Extended Data Fig. 2b) and near the surface (Extended Data Fig. 5), suggesting little risk of land pollution. Altogether, these results suggest that the targeted MCB intervention does not produce summertime climate effects far beyond the intervention zone outside the range of internal climate variability. Except for additional significant temperature responses over coastal Alaska, this conclusion is similar for MCB_{High} (not shown).

However, although aerosol emissions cease after September and the local wintertime SST response in the intervention zone is near-zero (Fig. 1b-c), ocean cooling persists to the south of the intervention zone into winter 2019-2020 resulting in some detectable remote wintertime climate effects (Fig. 6a & d). For example, the December-January-February (DJF) average near-surface air temperature response shows a small but statistically significant cooling south of the intervention zone in the stratocumulus deck and over continental North America. A significant wintertime response and an insignificant summertime response over North America is perhaps unsurprising given that atmospheric teleconnections are stronger in winter than summer [46] and past studies have shown an influence of wintertime North Pacific SSTs on North American temperatures [42]. In addition, stronger wintertime zonal winds may advect the temperature signal onshore. The $\sim 1°$C magnitude of this cooling would result in North American wintertime land temperature anomalies comparable or slightly smaller to those associated with a La Niña event [46]. However, DJF precipitation and geopotential height responses do not show coherent downstream impacts (Fig. 6b-c & e-f). Thus, limited remote wintertime impacts, primarily in the form of cooler temperatures approximately of the magnitude of internal variability, do occur directly downstream of this summertime MCB intervention.

4 Discussion

Here, we present the first work that explores whether a short-term, localized MCB intervention can mitigate the negative local impacts of a short-term (seasonal-to-annual) extreme MHW event. Using the summer 2019 Northeast Pacific Blob 2.0 as a case study, our results suggest that extreme summertime MHW events could potentially be mitigated without major remote impacts. The relative lack of significant

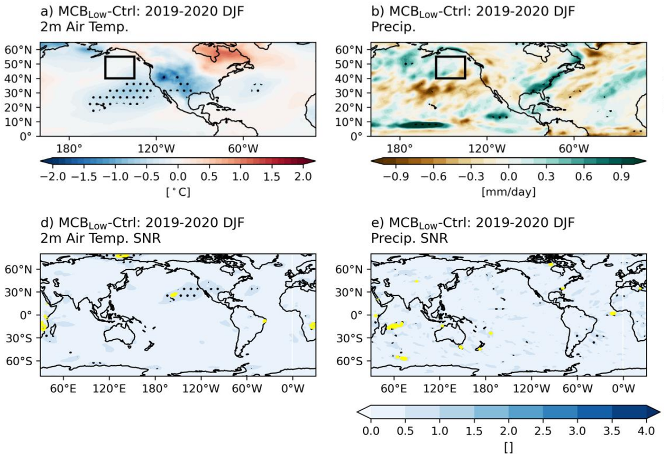

Fig. 6 Top row: 2019-2020 December-January-February (DJF) $\mathrm{MCB_{Low}}$-Ctrl difference in a) 2m air temperature, b) precipitation, and c) 500 hPa geopotential height (Z). Stippled regions are significant with 95% confidence. Black rectangles denote the intervention zone region in the Gulf of Alaska over which the MCB intervention is applied. Bottom row: Global map of DJF $\mathrm{MCB_{Low}}$-Ctrl signal-to-noise ratio (SNR) for d) 2m air temperature, e) precipitation, and f) 500 hPa Z. Stippled regions are significant with 95% confidence. The SNR = 1 contour is highlighted in yellow.

effects beyond the intervention zone represents an important difference between this work and other climate intervention studies that were aimed at mitigating global planetary-scale climate change through long-term interventions [24–28]. A previous study [34] using the same GCM and a similar MCB methodology shows that a longer (decadal-scale) emission period does produce a response in the tropical Pacific that, in turn, results in global-scale climate effects through teleconnections. That our MCB intervention does not show a similar response is thus primarily due to the limited scope (seasonal-to-yearlong) and scale (regional) of the aerosol emissions.

We acknowledge there could be lagged climate effects that appear in response to the MCB intervention beyond the length of our simulations. While intervention zone temperature responses are near-zero by DJF, temperatures in the stratocumulus deck remain anomalously cool enough to excite wintertime teleconnections to affect North America (Fig. 6a). Beyond winter, subtropical SST anomalies in the cloud deck could be communicated to the tropics via the wind-evaporation-SST feedback [40], potentially affecting global climate. In the subsurface, DJF potential temperature anomalies mostly remain within the climatological mixed layer (Extended Data Fig. 7a). If these anomalies subduct into the thermocline in late winter, however, they could be communicated to the tropics via the subtropical cells to affect equatorial thermocline temperatures [47].

Of course, remote effects likely depend on the strength and location of the MCB intervention, which in turn is affected by the accuracy of the MHW prediction. While the magnitude of the observed Blob 2.0 was within the forecast ensemble spread, it was substantially higher than the ensemble mean. Here, though the $\mathrm{MCB_{Low}}$ intervention overcorrected the ensemble mean forecast MHW and resulted in anomalous cooling in the Northeast Pacific, some ensemble members remain anomalously warm and thus presumably have negligible remote impacts from MCB. Similarly, an even weaker MCB intervention designed to simply reduce the magnitude of the ensemble mean MHW (without causing anomalous cooling) may have even smaller remote impacts. This possibility motivates further study of MCB interventions targeted to mitigate specific forecast MHWs. In addition, this underlines the importance of testing these principles across a range of GCM architectures with differing sensitivities to sea salt aerosol fluxes and teleconnection strengths [33, 48].

Damages due to the Blob 1.0 and Blob 2.0 MHWs each totaled hundreds of millions of dollars due to the collapse of commercial fisheries alone [7, 11]. Whether mitigation of such MHWs with MCB becomes economically viable depends on a variety of factors including the development of high-output sprayer technology [49] and the costs associated with operating a large number of ships that can also generate the energy needed to run pumps and fans. While a full accounting is beyond the scope of this work, assuming 6×10^{15} to 6×10^{16} particles/s emission rates [approximately 10 to 100 times greater than current test spray systems, 50], the 0.0417 Tg per month ($\sim 3.57 \times 10^{19}$ particles/s) emission rate for $\mathrm{MCB_{Low}}$ would require operating 600 to 6000 sprayers at once (an order of magnitude less than Wan et al.'s [37] intervention). Beyond economic viability, however, the question of whether to pursue such an approach to mitigate future MHWs (or other predictable extreme events) through localized and temporary interventions hinges on our confidence that it can be done safely and effectively. Altogether, our results motivate further study of this promising intervention approach.

5 Methods

5.1 Observed Sea Surface Temperature & Historical Damped Persistence

We consider monthly observed sea surface temperatures from January 1980 through December 2020 from the National Oceanographic and Atmospheric Administration National Center for Environmental Prediction (NOAA NCEP) Global Ocean Data Assimilation System (GODAS: [38]). Anomalies are taken relative to corresponding 1980-2018 monthly climatologies (i.e., prior to the Blob 2.0 event).

To calculate historical damped persistence of observed regional SST anomalies, we calculate the regional Pearson correlation coefficient of 1980-2018 GODAS SST anomalies which proceed an April SST anomaly at monthly lags. We select April 2019 as our damped persistence forecast initialization month because it is prior to the formation of the summertime Blob 2.0 MHW. We then multiply this time series of correlations by the April 2019 SST anomaly to create an estimate of historical damped persistence.

5.2 CESM2 SMYLE Simulations

To predict the observed 2019 summertime Northeast Pacific Blob 2.0 MHW, we re-run a 20-member initial condition ensemble initialized on May 1, 2019 of the Community Earth System Model, version 2 Seasonal-to-Multiyear Large Ensemble (CESM2 SMYLE, [39]) on the United States National Science Foundation National Center for Atmospheric Research's Derecho supercomputer. SMYLE is a free-running 20-member initial condition ensemble with dynamic coupling between earth system components. This ensemble approach allows us to analyze both ensemble mean (forced responses) and ensemble spread (internal variability). May 1, 2019 atmospheric initial conditions for SMYLE are obtained by interpolating a high resolution atmospheric reanalysis onto CESM2's atmospheric grid; ocean and sea ice initial conditions are obtained from a forced-ocean-sea-ice configuration of CESM2 driven by surface boundary conditions from a similar atmospheric reanalysis product.

SMYLE is skillful at predicting ENSO [39], the Pacific Decadal Oscillation [51], and MHWs [23]. Our control ensemble ("Ctrl") consists of 20 members with round-off error atmospheric temperature differences initialized from Yeager et al.'s [39] May 1, 2019 restart files. To account for drift and trend within the predictability ensemble [52], any full-field response in this paper (i.e., not a difference between a forced ensemble and Ctrl) is presented as an anomaly relative to all original SMYLE simulations initialized on May 1 over the years of 1980 through 2018.

5.3 CESM2 MCB Simulations

We also run four 20-member ensembles initialized from the same restarts as Ctrl but with marine cloud brightening perturbations. In all three ensembles, MCB is applied using a previously published and analyzed CESM2 methodology [33, 34, 48]. Briefly, these source code modifications apply a surface flux of accumulation-size mode sea salt aerosols in a specified region of the ocean. This MCB GCM methodology of direct aerosol emission is different than recent studies which instead perturb cloud droplet number [e.g., 31, 32, 37]. While our method may suffer from uncertainty in GCM parameterization of aerosol activation into cloud droplets, it includes direct aerosol effects such as shortwave scattering which are not included in cloud droplet number perturbation simulations.

We primarily discuss the results from i) an ensemble where a monthly flux of 0.0417 Tg of sea salt aerosol with volume radii of 47.1 nm is applied in the Gulf of Alaska intervention zone region of $40-50°$N, $155-135°$W from May 1, 2019 through September 30, 2019 ("MCB_{Low}" ensemble: total sea salt aerosol emission of 0.208 Tg). While models may substantially differ in their sensitivity to sea salt aerosol fluxes [33, 34, 48], we chose this forcing magnitude as it was five times weaker than Rasch et al.'s [33] specific guidance for a strong CESM2 response to MCB. We note that CESM2 is among the most sensitive GCMs to sea salt aerosol fluxes (and aerosol perturbations in general) and requires substantially lower aerosol masses to achieve the same radiative forcing as other GCMs [33, 48]. Thus, other models would likely require higher sea salt aerosol mass fluxes to simulate the same amount of radiative forcing and cooling to moderate the same MHW.

As sensitivity analyses, we also run ii) an ensemble with the same emissions magnitude as MCB_{Low} but extended through April 30, 2020 ("$\text{MCB}_{\text{LowExt}}$" ensemble: total sea salt aerosol emission of 0.5 Tg), iii) an ensemble with emissions from May 1, 2019 through September 30, 2019 but with an emissions magnitude 5× larger than MCB_{Low} ("MCB_{High}" ensemble: total sea salt aerosol emission of 1.04 Tg), and iv) an ensemble with the same emissions magnitude as MCB_{High} but extended through April 30, 2020 ("$\text{MCB}_{\text{HighExt}}$" ensemble: total sea salt aerosol emission of 2.5 Tg).

5.4 Marine Heatwave Definition

We define a marine heatwave as a monthly SST anomaly above the local 90^{th} percentile of a seasonally-dependent climatology [22]. We calculate the 90^{th} percentile for a certain region in SMYLE by considering all of the original SMYLE SST anomalies [39] from simulations initialized on May 1 over the period of 1980 through 2018. While the definition of a MHW strongly depends on climatological baseline choice [2], our definition of MHW is used for purely diagnostic purposes throughout this work.

5.5 Ocean Heat Budget

We perform a surface ocean heat budget where net surface heat flux (Q_{net}) is a sum of net surface shortwave radiation (SW), net surface longwave radiation (LW), and turbulent heat fluxes due to latent heat (LHF) and sensible heat (SHF):

$$Q_{net} = \text{SW} + \text{LW} + \text{LHF} + \text{SHF} \ . \tag{1}$$

All heat fluxes are defined as positive downward with units of Wm^{-2} and output by CESM2's atmospheric model.

Changes in Q_{net} are associated with changes in ocean heat storage (OHS), the time tendency of the ocean column's vertically-integrated heat content (OHC),

$$\text{OHS} = \frac{\partial}{\partial t}\text{OHC} = \rho_0 C_p \frac{\partial}{\partial t} \int_{-H}^{0} \theta \, dz \ , \tag{2}$$

as well as changes in the ocean column's horizontal heat flux divergence (OHD). In Equation (2), ρ_0 is a constant reference seawater density, C_p is the heat capacity of seawater, $-H$ is the full-depth of the ocean column, and θ is potential temperature as a function of time and space output by CESM2's ocean model. In Fig. 3, $Q_{net} \approx \text{OHS}$, suggesting that changes in ocean heat storage balance changes in net surface heat fluxes. The relatively small residuals between Q_{net} and OHS are a result of both OHD and other simplifying assumptions.

5.6 Statistical Significance and Signal-to-Noise Ratio

We test for statistical significance between the Ctrl and MCB ensembles using a Welch's two-sample t-test. This analysis tests the null hypothesis that two means are similar without making any assumption of shared variance structure. We consider all values with a p-value of less than 0.05 as statistically significant (i.e., significant at the 95% confidence level).

We also calculate the Signal-to-Noise (SNR) ratio with pooled variance as a diagnostic,

$$\text{SNR} = \left|\frac{\text{S}}{\text{N}}\right| = \left|\frac{\mu_{MCB} - \mu_{Ctrl}}{\sqrt{\left(\sum_n (x_{Ctrl,n} - \mu_{Ctrl})^2 + \sum_n (x_{MCB,n} - \mu_{MCB})^2\right)/(2n-2)}}\right|, \quad (3)$$

where μ is the ensemble mean, n is the ensemble size (in the case of SMYLE $n = 20$), and x_n is the ensemble member.

Supplementary information. This manuscript does not have supplementary information. Please see Extended Data Figures.

Acknowledgements. MTL, EB-W, and AD gratefully acknowledge funding from the Collaborative Research in Earth System Science and Technology program through the Funds for Science and Technology Foundation that spurred this project. In addition, MTL was supported by the Cooperative Institute for Climate, Ocean, & Ecosystem Studies (CICOES) under NOAA Cooperative Agreement NA20OAR4320271, Contribution No. 2026-1588; EB-W and AD were supported by the CO_2 Foundation; KCA was supported by a Calvin Professorship in Oceanography; and HH was supported by SilverLining's Safe Climate Research Initiative and the University of Washington's Marine Cloud Brightening Research Program. We thank NSF NCAR for providing an exploratory allocation of core hours on the Derecho supercomputer with which to run our simulations. Without implying their endorsement, we thank Nan Rosenbloom and Steve Yeager for suggestions for re-running SMYLE on Derecho and Rob Wood for helpful discussions regarding technical feasibility.

Declarations

Funding. See Acknowledgments.

Conflict of interest/Competing interests. The authors declare no competing interests.

Ethics approval and consent to participate. Not applicable.

Consent for publication. Not applicable.

Data availability. GCM simulations will be uploaded to a Zenodo repository upon study publication. NOAA NCEP GODAS data was provided by the NOAA Physical Sciences Laboratory in Boulder, CO, USA.

Materials availability. Not applicable.

Code availability. Code to create figures will be uploaded to a Zenodo repository upon study publication.

Author contributions. Conceptualization: MTL, EB-W, KCA, AD; Methodology: MTL, HH, JTC; Data Analysis: MTL, EB-W, JTC, AD; Visualization: MTL; Writing - Original draft: MTL; Writing - Review & editing: MTL, EB-W, KCA, HH, JTC, AD

References

[1] Hobday, A. J. *et al.* A Hierarchical Approach to Defining Marine Heatwaves. *Progress in Oceanography* **141**, 227–238 (2016).

[2] Amaya, D. J. *et al.* Marine Heatwaves Need Clear Definitions So Coastal Communities Can Adapt. *Nature* **616**, 29–32 (2023).

[3] Smale, D. A. *et al.* Marine Heatwaves Threaten Global Biodiversity and the Provision of Ecosystem Services. *Nature Climate Change* **9**, 306–312 (2019).

[4] Cavole, L. M. *et al.* Biological Impacts of the 2013–2015 Warm-Water Anomaly in the Northeast Pacific: Winners, Losers, and the Future. *Oceanography* **29**, 273–285 (2016).

[5] Wyatt, A. M., Resplandy, L. & Marchetti, A. Ecosystem Impacts of Marine Heat Waves in the Northeast Pacific. *Biogeosciences* **19**, 5689–5705 (2022).

[6] Cheung, W. W. & Frölicher, T. L. Marine Heatwaves Exacerbate Climate Change Impacts for Fisheries in the Northeast Pacific. *Scientific reports* **10**, 6678 (2020).

[7] Free, C. M. *et al.* Impact of the 2014–2016 Marine Heatwave on US and Canada West Coast Fisheries: Surprises and Lessons from Key Case Studies. *Fish and Fisheries* **24**, 652–674 (2023).

[8] Mogen, S. C. *et al.* Ocean Biogeochemical Signatures of the North Pacific Blob. *Geophysical Research Letters* **49**, e2021GL096938 (2022).

[9] Kohlman, C. *et al.* Surface and Subsurface Biogeochemical Impacts of the 2019 Northeast Pacific Marine Heatwave. *Geophysical Research Letters* **52**, e2025GL115230 (2025).

[10] Ferrer, E. M. *et al.* Abundant Interactions and Feedbacks between Aquatic Deoxygenation and the Other Planetary Boundaries Suggest "Unsafe" Levels of Oxygen Loss with Far-Reaching Impacts. *Limnology and Oceanography* **71**, e70434 (2026).

[11] Smith, K. E. *et al.* Socioeconomic Impacts of Marine Heatwaves: Global Issues and Opportunities. *Science* **374**, eabj3593 (2021).

[12] Frölicher, T. L., Fischer, E. M. & Gruber, N. Marine Heatwaves under Global Warming. *Nature* **560**, 360–364 (2018).

[13] Oliver, E. C. *et al.* Longer and More Frequent Marine Heatwaves over the Past Century. *Nature Communications* **9**, 1324 (2018).

[14] Capotondi, A. *et al.* A Global Overview of Marine Heatwaves in a Changing Climate. *Communications Earth & Environment* **5**, 701 (2024).

[15] Deser, C. *et al.* Future Changes in the Intensity and Duration of Marine Heat and Cold Waves: Insights from Coupled Model Initial-Condition Large Ensembles. *Journal of Climate* **37**, 1877–1902 (2024).

[16] Scannell, H. A., Pershing, A. J., Alexander, M. A., Thomas, A. C. & Mills, K. E. Frequency of Marine Heatwaves in the North Atlantic and North Pacific since 1950. *Geophysical Research Letters* **43**, 2069–2076 (2016).

[17] Bond, N. A., Cronin, M. F., Freeland, H. & Mantua, N. Causes and Impacts of the 2014 Warm Anomaly in the NE Pacific. *Geophysical Research Letters* **42**, 3414–3420 (2015).

[18] Amaya, D. J., Miller, A. J., Xie, S.-P. & Kosaka, Y. Physical Drivers of the Summer 2019 North Pacific Marine Heatwave. *Nature Communications* **11**, 1903 (2020).

[19] Scannell, H. A., Johnson, G. C., Thompson, L., Lyman, J. M. & Riser, S. C. Subsurface Evolution and Persistence of Marine Heatwaves in the Northeast Pacific. *Geophysical Research Letters* **47**, e2020GL090548 (2020).

[20] Chen, Z., Shi, J., Liu, Q., Chen, H. & Li, C. A Persistent and Intense Marine Heatwave in the Northeast Pacific during 2019–2020. *Geophysical Research Letters* **48**, e2021GL093239 (2021).

[21] Kohlman, C. *et al.* The 2019 Marine Heatwave at Ocean Station Papa: A Multi-Disciplinary Assessment of Ocean Conditions and Impacts on Marine Ecosystems. *Journal of Geophysical Research: Oceans* **129**, e2023JC020167 (2024).

[22] Jacox, M. G. *et al.* Global Seasonal Forecasts of Marine Heatwaves. *Nature* **604**, 486–490 (2022).

[23] Cohen, J. T., Thompson, L., Maroon, E., Deppenmeier, A.-L. & Cai, C. Object-Based Evaluation of Seasonal-to-Multiyear Marine Heatwave Predictions. *Geophysical Research Letters* **52**, e2025GL115021 (2025).

[24] Latham, J. Control of Global Warming? *Nature* **347**, 339–340 (1990).

[25] Latham, J. Amelioration of Global Warming by Controlled Enhancement of the Albedo and Longevity of Low-Level Maritime Clouds. *Atmospheric Science Letters* **3**, 52–58 (2002).

[26] Latham, J. *et al.* Global Temperature Stabilization via Controlled Albedo Enhancement of Low-Level Maritime Clouds. *Philosophical Transactions of the Royal Society A: Mathematical, Physical and Engineering Sciences* **366**, 3969–3987 (2008).

[27] Jones, A., Haywood, J. & Boucher, O. Climate Impacts of Geoengineering Marine Stratocumulus Clouds. *Journal of Geophysical Research: Atmospheres* **114** (2009).

[28] Rasch, P. J., Latham, J. & Chen, C.-C. Geoengineering by Cloud Seeding: Influence on Sea Ice and Climate System. *Environmental Research Letters* **4**, 045112 (2009).

[29] Hill, S. & Ming, Y. Nonlinear Climate Response to Regional Brightening of Tropical Marine Stratocumulus. *Geophysical Research Letters* **39** (2012).

[30] Latham, J. *et al.* Marine Cloud Brightening: Regional Applications. *Philosophical Transactions of the Royal Society A: Mathematical, Physical, and Engineering Sciences* **372**, 20140053 (2014).

[31] Hirasawa, H., Hingmire, D., Singh, H., Rasch, P. J. & Mitra, P. Effect of Regional Marine Cloud Brightening Interventions on Climate Tipping Elements. *Geophysical Research Letters* **50**, e2023GL104314 (2023).

[32] Wan, J. S. *et al.* Diminished Efficacy of Regional Marine Cloud Brightening in a Warmer World. *Nature Climate Change* **14**, 808–814 (2024).

[33] Rasch, P. J. *et al.* A Protocol for Model Intercomparison of Impacts of Marine Cloud Brightening Climate Intervention. *Geoscientific Model Development* **17**, 7963–7994 (2024).

[34] Hirasawa, H. *et al.* Forcing Susceptibility and Climate Sensitivity to Midlatitude Marine Cloud Brightening. *Journal of Climate* **39**, 769–784 (2026).

[35] Krantz, W., Neelin, J. D. & Ahmed, F. A Framework for Minimizing Remote Effects of Regional Climate Interventions: Cooling the Great Barrier Reef without Teleconnections. *Geophysical Research Letters* **52**, e2024GL113191 (2025).

[36] Henry, M., Hirasawa, H., Haywood, J. & Rasch, P. J. Marine Cloud Brightening to Cool the Arctic: An Earth System Model Comparison. *Earth's Future* **13**, e2025EF006508 (2025).

[37] Wan, J. S., Fasullo, J. T., Rosenbloom, N., Chen, C.-C. & Ricke, K. Targeted Marine Cloud Brightening Weakens Subsequent El Niño. *Science Advances* **12**, eadx3012 (2026).

[38] Behringer, D. W., Ji, M. & Leetmaa, A. An Improved Coupled Model for ENSO Prediction and Implications for Ocean Initialization. Part I: The Ocean Data Assimilation System. *Monthly Weather Review* **126**, 1013–1021 (1998).

[39] Yeager, S. G. *et al.* The Seasonal-to-Multiyear Large Ensemble (SMYLE) Prediction System Using the Community Earth System Model version 2. *Geoscientific*

Model Development Discussions **2022**, 1–42 (2022).

[40] Luongo, M. T., Xie, S.-P., Eisenman, I., Hwang, Y.-T. & Tseng, H.-Y. A Pathway for Northern Hemisphere Extratropical Cooling to Elicit a Tropical Response. *Geophysical Research Letters* **50**, e2022GL100719 (2023).

[41] Eddebbar, Y. A. *et al.* El Niño–like Physical and Biogeochemical Ocean Response to Tropical Eruptions. *Journal of Climate* **32**, 2627–2649 (2019).

[42] Hartmann, D. L. Pacific Sea Surface Temperature and the Winter of 2014. *Geophysical Research Letters* **42**, 1894–1902 (2015).

[43] Di Lorenzo, E. & Mantua, N. Multi-Year Persistence of the 2014/15 North Pacific Marine Heatwave. *Nature Climate Change* **6**, 1042–1047 (2016).

[44] Tseng, Y.-H., Ding, R. & Huang, X.-m. The Warm Blob in the Northeast Pacific—The Bridge Leading to the 2015/16 El Niño. *Environmental Research Letters* **12**, 054019 (2017).

[45] Odoulami, R. C. *et al.* Africa's Climate Response to Marine Cloud Brightening strategies is Highly Sensitive to Deployment Region. *Journal of Geophysical Research: Atmospheres* **129**, e2024JD041070 (2024).

[46] Deser, C., Simpson, I. R., Phillips, A. S. & McKinnon, K. A. How Well Do We Know ENSO's Climate Impacts over North America, and How Do We Evaluate Models Accordingly? *Journal of Climate* **31**, 4991–5014 (2018).

[47] Luongo, M. T., Xie, S.-P., Eisenman, I., Sun, S. & Peng, Q. How the Subsurface Tropical Pacific Responds to Subtropical Surface Cooling: Implications for Cross-Equatorial Transport. *Journal of Climate* **38**, 3313–3331 (2025).

[48] Hirasawa, H. *et al.* G6-1.5 K-MCB: Marine Cloud Brightening Scenario Design for the Geoengineering Model Intercomparison Project (GeoMIP) in CESM2.1, E3SMv2.0, and UKESM1.1. *Geoscientific Model Development* **19**, 3257–3283 (2026).

[49] Wood, R. Assessing the Potential Efficacy of Marine Cloud Brightening for Cooling Earth using a Simple Heuristic Model. *Atmospheric Chemistry and Physics* **21**, 14507–14533 (2021).

[50] Hernandez-Jaramillo, D. C. *et al.* First Generation Outdoor Marine Cloud Brightening Trial Increases Aerosol Concentration at Cloud Base Height. *Environmental Research Letters* **20**, 054065 (2025).

[51] Meeker, E. *et al.* Seasonality of Pacific Decadal Oscillation Prediction Skill. *Geophysical Research Letters* **52**, e2025GL116122 (2025).

[52] Meehl, G. A. *et al.* The Effects of Bias, Drift, and Trends in Calculating Anomalies for Evaluating Skill of Seasonal-to-Decadal Initialized Climate Predictions. *Climate Dynamics* **59**, 3373–3389 (2022).

Extended Data

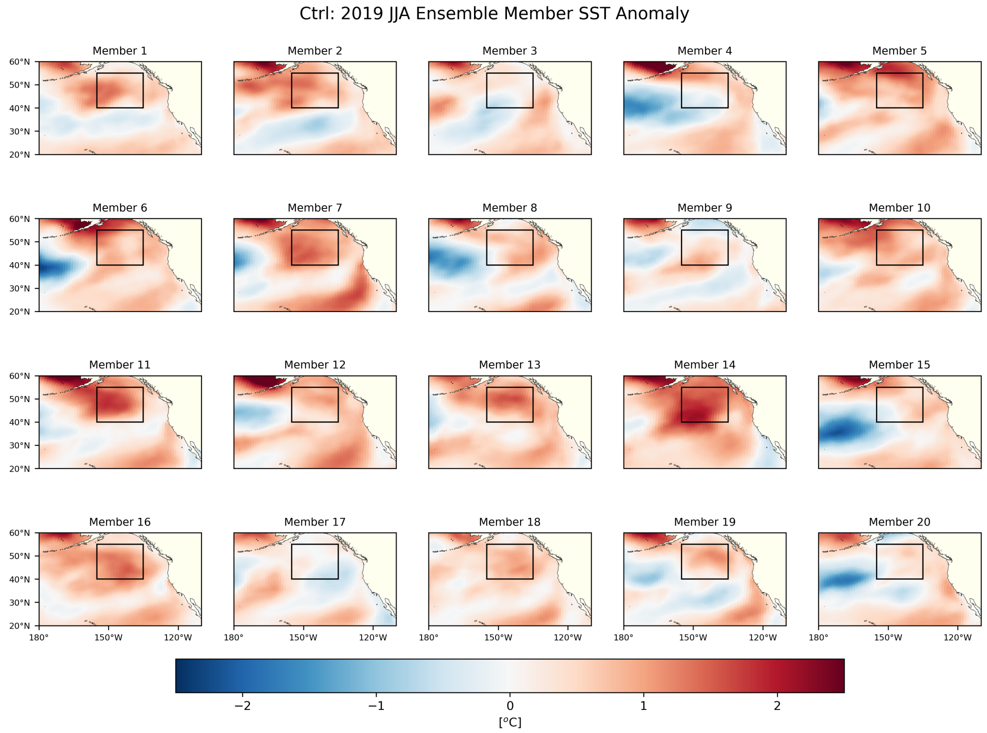

Extended Data Figure 1 2019 June-July-August (JJA) sea surface temperature (SST) anomaly for each ensemble member of Ctrl. Anomalies are calculated relative to all SMYLE simulations initialized on May 1 from 1980 through 2018. Black rectangles denote the intervention zone region in the Gulf of Alaska over which the MCB intervention is applied, which in turn is based on the ensemble mean location of maximum SST anomalies in this ensemble (Fig. 2a).

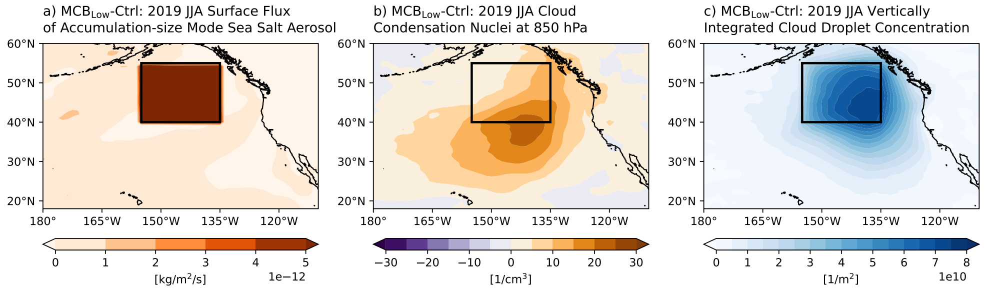

Extended Data Figure 2 2019 June-July-August (JJA) MCB$_{\text{Low}}$-Ctrl difference in a) the surface flux of accumulation-size mode sea salt aerosol, b) cloud condensation nuclei at the 850 hPa vertical level, and e) vertically integrated cloud droplet concentration. Black rectangles denote the intervention zone region in the Gulf of Alaska over which the MCB intervention is applied.

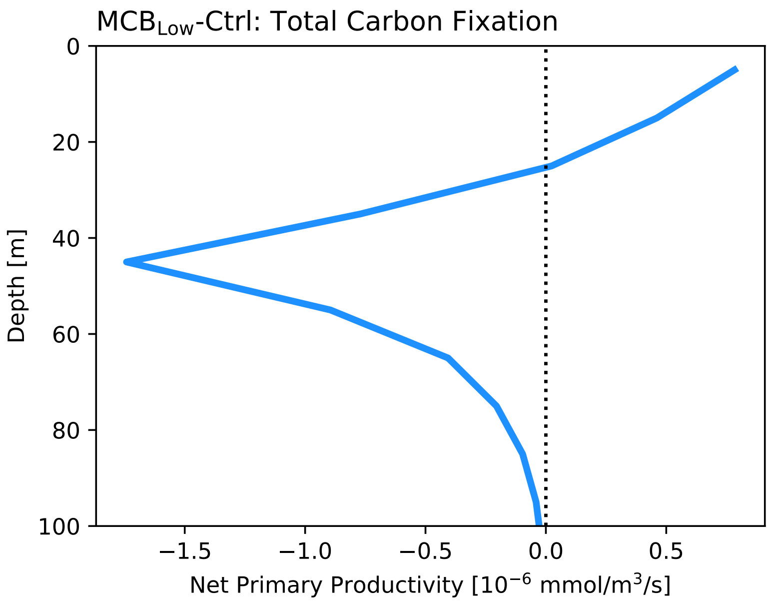

Extended Data Figure 3 2019 June-July-August (JJA) MCB$_{\text{Low}}$-Ctrl Gulf of Alaska area-averaged (40 − 55°N, 155 − 135°W) depth profile of total carbon fixation by phytoplankton via photosynthesis (i.e., net primary productivity: NPP).

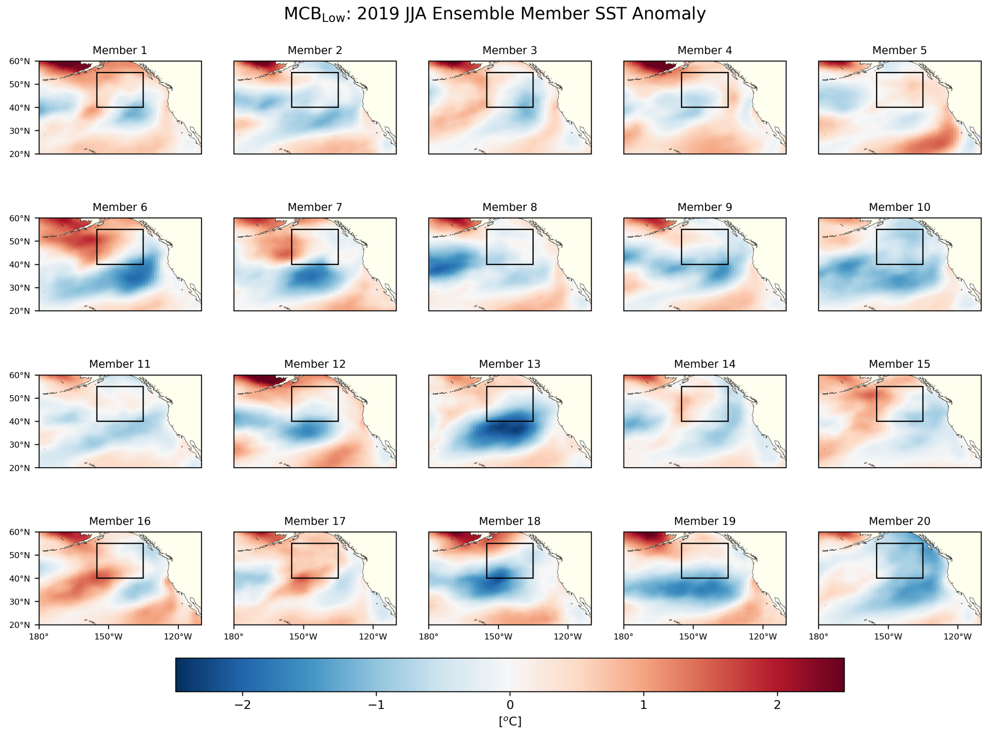

Extended Data Figure 4 2019 June-July-August (JJA) sea surface temperature (SST) anomaly for each ensemble member of MCB$_{Low}$. Anomalies are calculated relative to all SMYLE simulations initialized on May 1 from 1980 through 2018. Black rectangles denote the intervention zone region in the Gulf of Alaska over which the MCB intervention is applied.

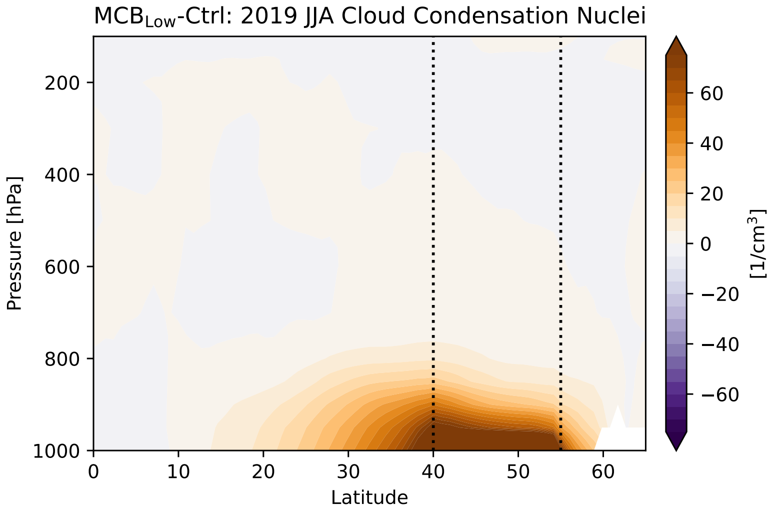

Extended Data Figure 5 2019 June-July-August (JJA) MCB$_{\text{Low}}$-Ctrl zonally-averaged (155 − 135°W) vertical atmospheric profile of cloud condensation nuclei. Dotted vertical lines denote the Gulf of Alaska intervention zone latitudes.

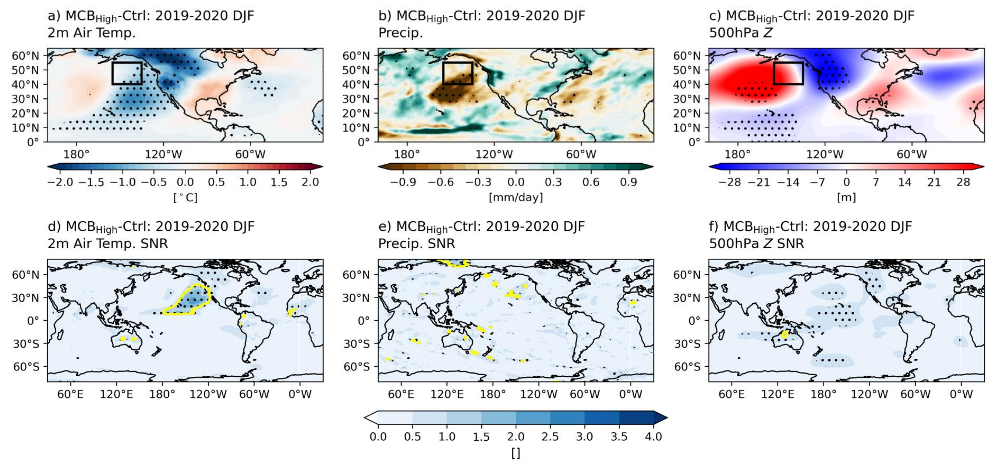

Extended Data Figure 6 Top row: 2019-2020 December-January-February (DJF) MCB$_{\text{High}}$-Ctrl difference in a) 2m air temperature, b) precipitation, and c) 500 hPa geopotential height (Z). Stippled regions are significant with 95% confidence. Black rectangles denote the intervention zone region in the Gulf of Alaska over which the MCB intervention is applied. Bottom row: Global map of DJF MCB$_{\text{High}}$-Ctrl signal-to-noise ratio (SNR) for d) 2m air temperature, e) precipitation, and f) 500 hPa Z. Stippled regions are significant with 95% confidence. The SNR = 1 contour is highlighted in yellow.

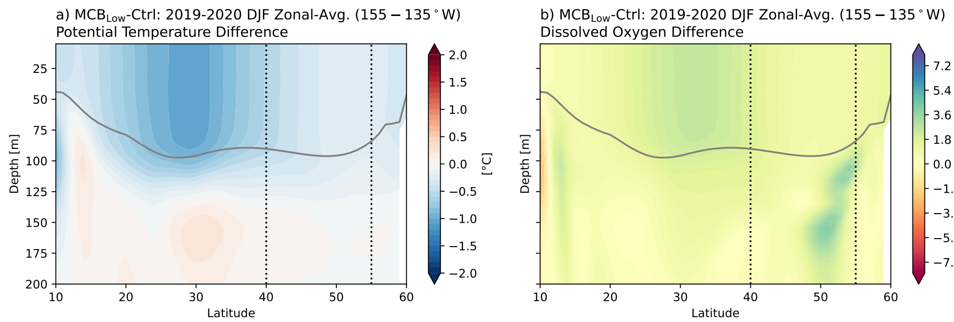

Extended Data Figure 7 2019-2020 December-January-February (DJF) MCB$_{\text{Low}}$-Ctrl difference in subsurface zonally-averaged ($155 - 135°$W) a) potential temperature and b) dissolved oxygen. The solid gray line is the DJF climatological mixed layer depth calculated from SMYLE over 1980-2018. Dotted vertical lines denote the Gulf of Alaska intervention zone latitudes.